CIDER 2006 Summer Program

Mineral Physics Component

Min Phys I Thermodynamics (Lars)

Min Phys 2 Mantle Mineralogy (Lars)

Tutorial 1 Constructing Earth Models (Lars)

Tutorial 2 Melts (Marc)

Min Phys 3 Equation of state and Lattice Dynamics (Tom)

Min Phys 4 Phase Equilibria (Marc)

→ Min Phys 5 Elasticity (Tom)

Tutorial 3 Equation of state data analysis (Tom)

Min Phys 6 Fluids and Melts (Marc)

Elasticity: Understanding mantle structure and composition

Upper Mantle Seismic Velocity Structure

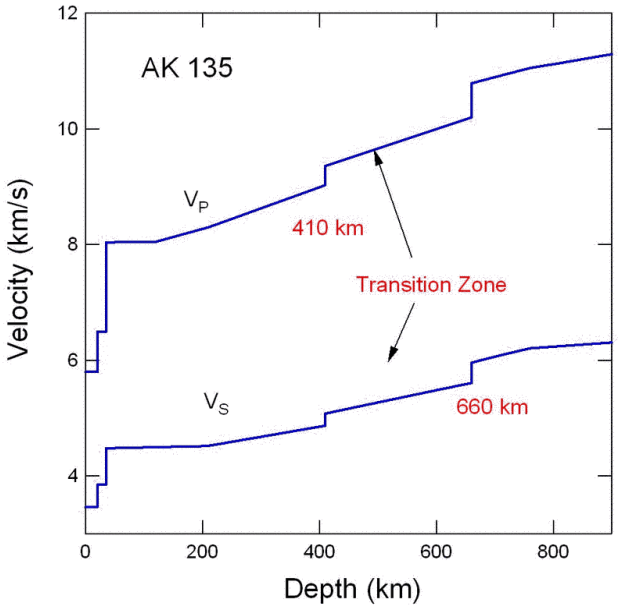

Velocity Variation

--Pressure

--Temperature

-- Phase (Structure)

--Composition

Discontinuity Properties

--Depth

--Amplitude

--Width

--Fine Structure

Seismic tomography of the mantle: What happens to subducting slabs?

"Stagnant Slabs"

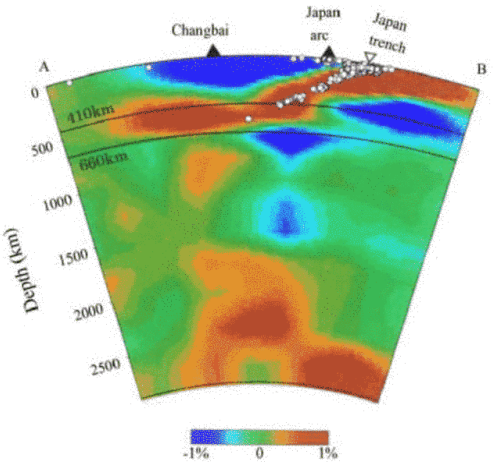

Note: Reversed color scheme

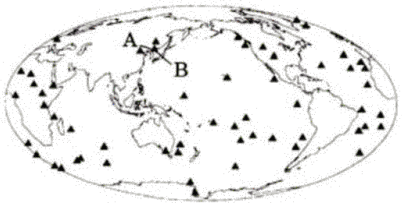

Zhao, 2004

Elasticity

Hooke's Law: $\sigma_{ij} = C_{ijkl}\varepsilon_{kl}$ i,j,k,l = 1,2,3

Stress tensor — Strain tensor

C_{ijkl} = elastic stiffness tensor (81 terms)

By symmetry, $C_{ijkl} = C_{ijlk}$ and $C_{ijkl} = C_{jikl}$

81 terms → reduced to 36 terms or 6 x 6 matrix.

In reduced notation: $\sigma_i = C_{ij}\varepsilon_j$ i,j = 1,…,6

Crystal system	# of C_{ij}s
Triclinic	21
Monoclinic	13
Orthorhombic	9
Tetragonal	6 or 7
Hexagonal	5
Cubic	3
Isotropic	2

What do the C_{ij} mean?

C_{ii}	i=1,2,3	relate a compressional stress to a compressional strain both in the same direction
C_{ii}	i=4,5,6	relates a shear stress to a shear strain, both in the same plane
C_{ij}	I,j=1,2,3	relates a compressional stress to a perpendicular compressional strain
C_{ij}	I,j=4,5,6	relates a shear stress to a perpendicular shear strain

Elastic Moduli: A Mineral Physics Perspective

--related on a microscopic level to interatomic forces. (i.e. shape of intermolecular potential)

-- most direct means to obtain the bulk modulus (and other aggregate properties) through suitable averaging of the single crystal properties.

-- related on a macroscopic level to the bulk mechanical (particularly shear) properties of a crystal. (e.g. Hardness)

--moduli as a function of pressure and temperature can be sensitive indicators of phase transitions and their mechanisms. ("Shear softening")

-- elastic properties are the best constrained properties of Earth's interior.

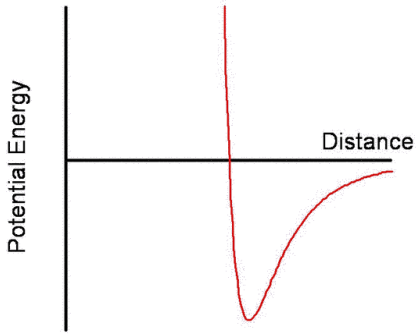

Brillouin scattering

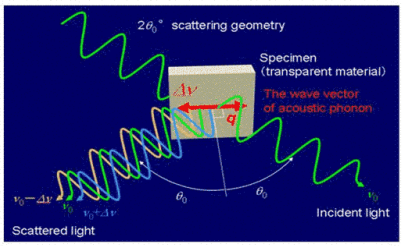

(From Shimizu and Sasaki)

Stokes: $\nu_S = \nu_i + \Delta\nu$

Anti-Stokes: $\nu_S = \nu_i - \Delta\nu$

From a quantum point of view, Brillouin scattering is considered to consist of interaction of photons with acoustic or vibrational phonons.

$$V = \frac{\Delta\nu\ \lambda_0}{2\sin(\theta/2)}$$

V: acoustic velocity

λ_0 : incident wavelength

θ: scattering angle (70^0 in this study)

Brillouin Scattering in the Diamond Anvil Cell

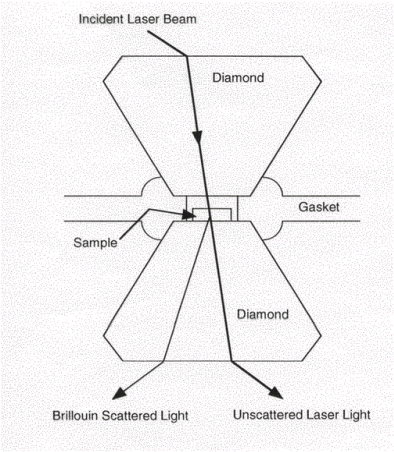

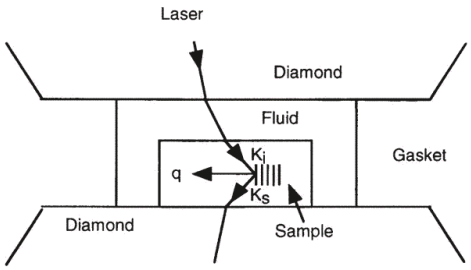

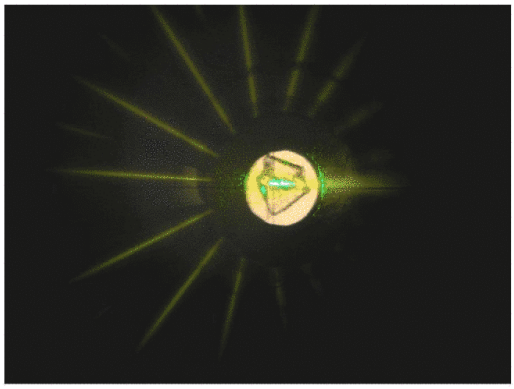

$$V = \frac{\Delta \nu \lambda_0}{2\sin(\theta_0/2)}$$

Elasticity of fayalite (Fe_2SiO_4) to 12 GPa

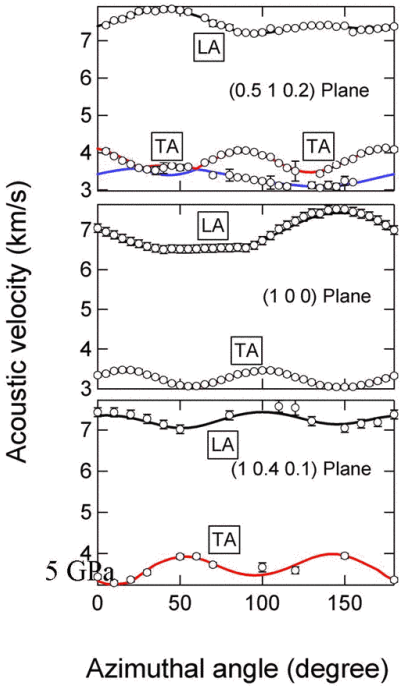

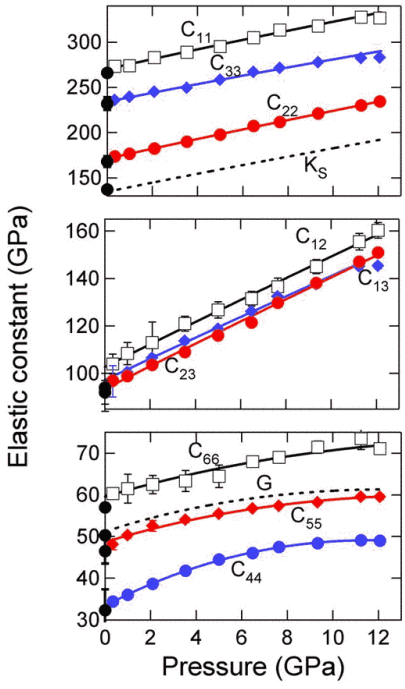

Speziale, Duffy, and Angel, *JGR*, 2004

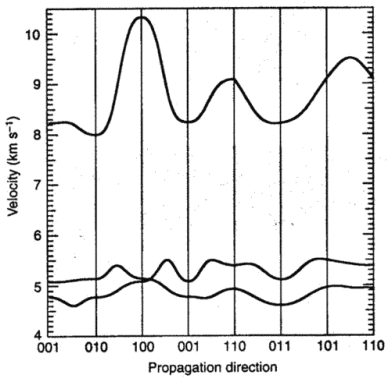

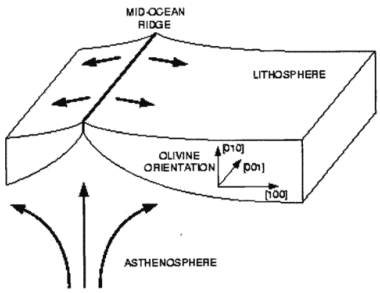

Fig. 2.1. Anisotropy of forsterite showing the *P*-wave (upper line) and *S*-wave (lower lines) velocities as a function of propagation direction; from the LDA pseudo-potential calculations of [65].

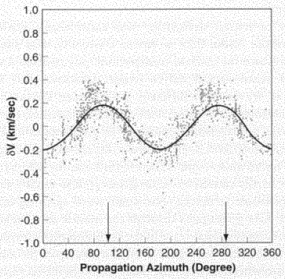

Fig. 3-6. The first observation of upper-mantle anisotropy (after Raitt et al. 1969). The graph shows the compressional wave velocity propagating through the uppermost mantle beneath the eastern Pacific as a function of the propagation azimuth. The fastest azimuths (shown by arrows) are parallel to the direction of plate motion.

Elasticity of Isotropic solids

Isotropic – liquid, glass, randomly oriented aggregates of anisotropic minerals

2 elastic moduli can fully describe isotropic minerals:

Lame constants (λ) and (μ)

Young's modulus (E) and Poisson's ration (ν)

Bulk modulus (K) and Shear modulus (μ or G)

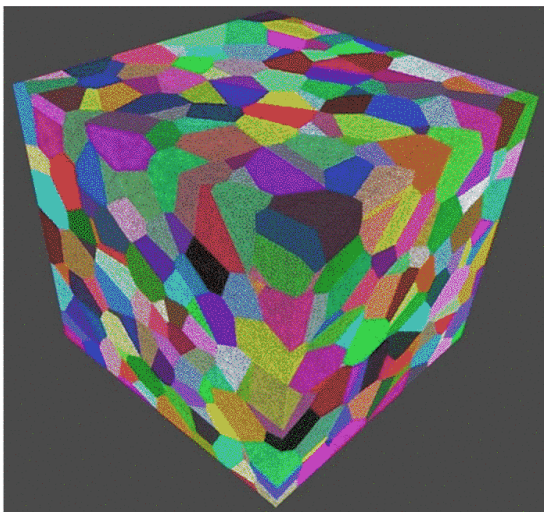

Aggregate seismic wave velocities:

Shear (β): $\rho V_S^2 = G = \mu = \frac{1}{2}(C_{11} - C_{12})$

Compressional (α):

$$\rho V_P^2 = K + \frac{4}{3}G = \lambda + 2\mu = C_{11}$$

Bulk: $\rho V_B^2 = K = \lambda + \frac{2}{3}\mu = \frac{1}{3}(C_{11} + 2C_{12})$

Elastic Properties at deep mantle conditions

"Hot" finite strain isotherms:

$$V_0(T) = V_0(T_0)\exp\int_{T_0}^{T}\alpha(T)dT$$

$$\alpha(T) = a + bT - \frac{c}{T^2}$$

$$K_{T0}(T) = K_{T0}(T_0) + \left(\frac{\partial K_T}{\partial T}\right)_P (T - T_0)$$

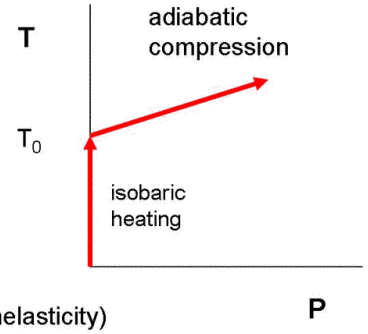

with a similar expression for $K_{S0}(T)$, $G_0(T)$. (+ anelasticity)

Third order finite strain equations:

$$K = (1+2f)^{5/2} K_0 [1 + (3K_0' - 5)f]$$

$$G = (1+2f)^{5/2} G_0 \left[1 + (3\frac{K_0}{G_0}G_0' - 5)f\right]$$

$$P = \frac{3K_{T0}}{2}\left[\left(\frac{V_0}{V}\right)^{7/3} - \left(\frac{V_0}{V}\right)^{5/3}\right]\left\{1 - \frac{3}{4}\left(4 - K_{T0}'\right)\left[\left(\frac{V_0}{V}\right)^{2/3} - 1\right]\right\}$$

$$\frac{\rho}{\rho_0} = \frac{V_0}{V} = (1+2f)^{3/2}$$

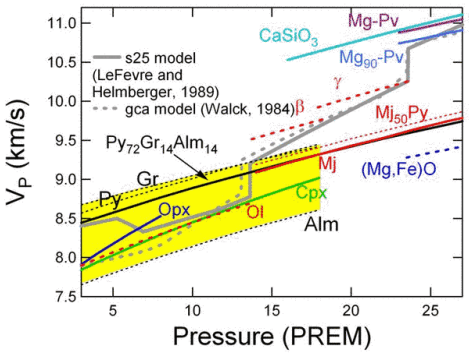

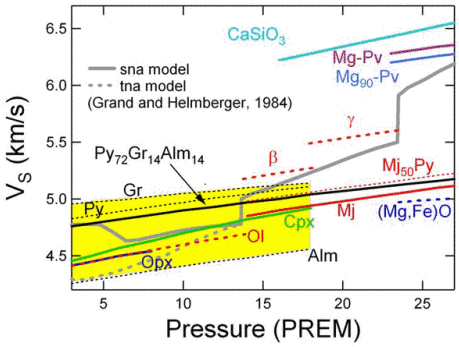

S. Speziale, unpublished

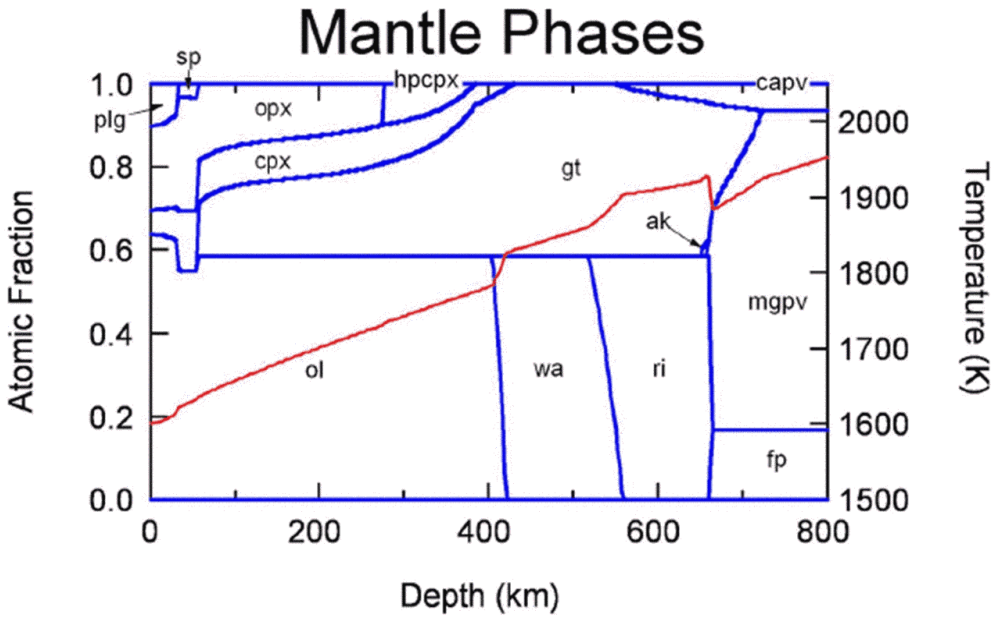

Wadsleyite (wa); Ringwoodite (ri); akimotoite (ak); Mg-perovskite (mgpv); Ca-perovskite (capv); Ferropericlase (fp)

Major element composition of the upper mantle

Table 2.1. Different models for the major-element composition of the bulk silicate Earth (primitive Mantle)

	Ringwood (1975)	Ringwood (1979)	Jagoutz et al. (1979)	Wanke et al. (1984)	Palme and Nickel (1985)	Hart and Zindler (1986)	McDonough and Sun (1995)	O'Neill and Palme (1998)	McDonough & Sun	Sun (1982)
MgO	38.1	38.1	38.3	36.8	35.5	37.8	37.8	36.33	37.81	38
Al2O3	4.6	3.3	4.0	4.1	4.8	4.1	4.4	4.73	4.44	4.3
SiO2	45.1	45.1	45.1	45.6	46.2	46	45	45.56	44.93	
CaO	3.1	3.1	3.5	3.5	4.4	3.2	3.5	3.75	3.54	3.5
FeO	7.9	8	7.8	7.5	7.7	7.5	8.1	8.17	8.05	8.4
Total	98.8	97.6	98.7	97.5	98.6	98.6	98.8	98.54	98.77	54.2
Mg#	0.896	0.895	0.897	0.897	0.891	0.899	0.893	0.888	0.89	0.890

Pyrolite: Ringwood's term for primary fertile mantle

~3 parts peridotite + 1 part basalt

Pyrolite mineral proportions

Olivine	(Mg,Fe)2SiO4	57 wt. %
Ortho**pyroxene**	(Mg, Fe)SiO3	17 wt. %
Clino**pyroxene**	(Ca,Mg,Fe)SiO3	12 wt. %
Garnet	(Mg,Fe,Ca)3(Al,Cr)2Si3O12	14 wt. %

Stixrude and Lithgow-Bertelloni, GJI, 2004

Table 1. Properties of mantle species.

Phase	Species	Formula	V_0 $cm^3\ mol^{-1}$	K_0 GPa	K_0'	θ_0 K	γ_0	q	G_0 GPa	G_0'	η_{S0}	Ref.
Feldspar (plg)	Anorthite	$CaAl_2Si_2O_8$	100.61	84 (5)	*4.0* (10)	752 (2)	0.39 (5)	*1.0* (10)	40 (3)	*1.1* (5)	*1.6* (10)	1-5
Spinel (sp)	Spinel	$(Mg_3Al)(Al_7Mg)O_{16}$	159.05	197 (1)	5.7 (2)	900 (3)	1.02 (4)	2.8 (6)	109 (10)	0.4 (5)	2.7 (6)	1,4,6-8
Spinel	Hercynite	$(Fe_3Al)(Al_7Fe)O_{16}$	163.37	209 (2)	*5.7* (10)	768 (23)	1.21 (7)	*2.8* (10)	85 (13)	*0.4* (5)	*2.8* (10)	1,2,9,10
Olivine (ol)	Forsterite	Mg_2SiO_4	43.60	128 (2)	4.2 (2)	809 (1)	0.99 (3)	2.1 (2)	82 (2)	1.4 (1)	2.4 (1)	1,8,11-13
Olivine	Fayalite	Fe_2SiO_4	46.29	135 (2)	4.2 (10)	619 (2)	1.06 (7)	3.6 (10)	51 (2)	*1.4* (5)	1.1 (6)	1,2,4,5,8,14,15
Wadsleyite (wa)	Mg-Wadsleyite	Mg_2SiO_4	40.51	169 (3)	4.3 (2)	*881* (100)	1.22 (9)	2.0 (10)	112 (2)	1.4 (2)	2.7 (4)	1,5,16-19
Wadsleyite	Fe-Wadsleyite	Fe_2SiO_4	43.21	169 (13)	*4.3* (10)	*599* (100)	*1.22* (30)	*2.0* (10)	72 (12)	*1.4* (5)	*1.1* (10)	16,20
Ringwoodite (ri)	Mg-Ringwoodite	Mg_2SiO_4	39.49	183 (2)	4.1 (2)	*908* (100)	1.10 (10)	2.8 (4)	120 (2)	1.3 (1)	2.7 (5)	1,5,16,21
Ringwoodite	Fe-Ringwoodite	Fe_2SiO_4	42.03	218 (7)	*4.1* (10)	*685* (100)	1.30 (24)	*2.8* (10)	95 (10)	*1.3* (5)	*1.9* (10)	1,16,21,22
Orhopyroxene (opx)	Enstatite	$Mg_4Si_4O_{12}$	125.35	107 (2)	7.1 (4)	810 (8)	0.67 (4)	7.8 (11)	77 (1)	1.6 (1)	2.4 (5)	1,23-29
Orthopyroxene	Ferrosilite	$Fe_4Si_4O_{12}$	131.88	101 (4)	7.1 (5)	680 (16)	0.67 (8)	*7.8* (10)	52 (5)	*1.6* (5)	*1.1* (10)	1,2,9,23,30,31
Orthopyroxene	Mg-Tschermak's	$(Mg_2Al_2)Si_2Al_2O_{12}$	120.50	*107* (10)	*7.1* (10)	*856* (100)	*0.67* (30)	*7.8* (10)	*88* (10)	*1.6* (5)	*2.4* (10)	32
Clinopyroxene (cpx)	Diopside	$CaMg_2Si_4O_{12}$	132.08	112 (5)	5.2 (18)	782 (5)	0.96 (5)	1.5 (20)	67 (2)	*1.4* (5)	*1.6* (10)	1,2,5,26,33,34
Clinopyroxene	Hedenbergite	$CaFe_2Si_4O_{12}$	135.73	119 (4)	5.2 (10)	702 (4)	0.93 (6)	*1.5* (10)	61 (1)	*1.2* (5)	*1.6* (10)	1,2,5,15,35
Clinopyroxene	Mg-Diopside	$Mg_2Mg_2Si_4O_{12}$	126.00	*112* (10)	*5.2* (10)	*851* (100)	*0.96* (30)	*1.5* (10)	*75* (10)	*1.5* (5)	*1.7* (10)	36
C2/c-pyroxene (C2/c)	HP-Clinoenstatite	$Mg_4Si_4O_{12}$	121.94	107 (26)	5.3 (40)	*768* (100)	0.95 (4)	1.1 (45)	*84* (10)	*1.8* (5)	*1.6* (10)	37
C2/c-pyroxene	HP-Clinoferrosilite	$Fe_4Si_4O_{12}$	128.10	*107* (10)	*5.3* (10)	*617* (100)	*0.95* (30)	*1.1* (10)	*70* (10)	*1.5* (5)	*1.4* (10)	38
Ca-perovskite (cpv)	Ca-Perovskite	$CaSiO_3$	27.45	236 (4)	3.9 (2)	*984* (100)	1.53 (7)	1.6 (16)	165 (12)	2.5 (5)	*2.4* (10)	1,39-41
Akimotoite (ak)	Mg-Akimotoite	$MgSiO_3$	26.35	211 (4)	4.5 (5)	*850* (100)	1.18 (13)	*1.3* (10)	132 (8)	1.6 (5)	*2.7* (10)	1,2,5,42
Akimotoite	Fe-Akimotoite	$FeSiO_3$	26.85	*211* (10)	*4.5* (10)	*810* (100)	*1.18* (30)	*1.3* (10)	*158* (10)	*1.6* (5)	*3.7* (10)	20
Akimotoite	Corundum	$AlAlO_3$	25.58	253 (5)	4.3 (2)	933 (3)	1.32 (4)	1.3 (2)	163 (2)	1.6 (1)	2.8 (2)	1,4,5,8,43
Garnet (gt,mj)	Pyrope	$Mg_3AlAlSi_3O_{12}$	113.08	170 (2)	4.1 (3)	823 (4)	1.01 (6)	1.4 (5)	94 (2)	1.3 (2)	1.0 (3)	1,4,44-46
Garnet	Almandine	$Fe_3AlAlSi_3O_{12}$	115.43	177 (3)	4.1 (3)	742 (5)	1.10 (6)	*1.4* (10)	98 (3)	*1.3* (5)	*2.2* (10)	1,9,45,47,48
Garnet	Grossular	$Ca_3AlAlSi_3O_{12}$	125.12	167 (1)	5.5 (4)	823 (2)	1.08 (6)	0.4 (4)	108 (1)	1.1 (2)	2.4 (2)	1,4,8,25,45,49,50
Garnet	Mg-Majorite	$Mg_3MgSiSi_3O_{12}$	114.32	165 (3)	4.2 (3)	*788* (100)	*1.01* (30)	1.4 (5)	85 (2)	1.4 (2)	0.7 (5)	1,46,51
Stishovite (st)	Stishovite	SiO_2	14.02	314 (8)	4.4 (2)	1044 (20)	1.34 (17)	2.4 (22)	220 (12)	*1.6* (5)	*5.0* (10)	1,4,5,52-54
Perovskite (pv)	Mg-Perovskite	$MgSiO_3$	24.45	251 (3)	4.1 (1)	*1070* (100)	1.48 (5)	1.4 (5)	175 (2)	1.7 (2)	2.6 (6)	1,55-58
Perovskite	Fe-Perovskite	$FeSiO_3$	25.48	281 (40)	*4.1* (10)	*841* (100)	*1.48* (30)	*1.4* (10)	138 (40)	*1.7* (5)	*2.1* (10)	20,59
Perovskite	Al-Perovskite	$AlAlO_3$	25.49	228 (10)	4.1 (5)	*1021* (100)	*1.48* (30)	*1.4* (10)	*160* (10)	*1.7* (5)	*3.0* (10)	60,61
Magnesiowüstite (mw)	Periclase	MgO	11.24	161 (3)	3.9 (2)	773 (9)	1.50 (2)	1.5 (2)	130 (3)	2.2 (1)	2.3 (2)	1,4,7,8,44
Magnesiowüstite	Wüstite	FeO	12.06	152 (1)	4.9 (2)	455 (12)	1.28 (11)	*1.5* (10)	47 (1)	0.7 (1)	*0.8* (10)	1,5,62-64

Italicized entries are from systematics. References: 1. Smyth & McCormick (1995) 2. Bass (1995) 3. Angel et al. (1988) 4. Robie & Hemingway (1995) 5. Fei (1995) 6. Yoneda (1990) 7. Fiquet et al. (1999) 8. Anderson & Isaak (1995) 9. Anovitz et al. (1993) 10. Harrison et al. (1998) 11. Zha et al. (1996) 12. Robie et al. (1982) 13. Bouhifd et al. (1996) 14. Zha et al. (1998) 15. Knittle (1995) 16. Sinogeikin et al. (1998) 17. Zha et al. (1997) 18. Fei et al. (1992) 19. Li et al. (2001) 20. Jeanloz & Thompson (1983) 21. Sinogeikin et al. (2001) 22. Mao et al. (1969) 23. Jackson et al. (1999) 24. Flesch et al. (1998) 25. Thieblot et al. (1999) 26. Krupka et al. (1985) 27. Jackson et al. (2003) 28. Zhao et al. (1995) 29. Frisillo & Barsch (1972) 30. HughJones & Angel (1997) 31. HughJones (1997) 32. Skinner & Boyd (1964) 33. Levien & Prewitt (1981) 34. Zhao et al. (1998) 35. Haselton et al. (1987) 36. Tribaudino et al. (2001) 37. Shinmei et al. (1999) 38. HughJones et al. (1996) 39. Shim et al. (2000) 40. Wang et al. (1996) 41. Karki & Crain (1998) 42. Dasilva et al. (1999) 43. Gieske & Barsch (1968) 44. Sinogeikin & Bass (2000) 45. Thieblot et al. (1998) 46. Sinogeikin & Bass (2002) 47. Sinogeikin et al. (1997) 48. Zhang et al. (1999) 49. Oneill et al. (1989) 50. Conrad et al. (1999) 51. Sinogeikin & Bass (2002) 52. Weidner et al. (1982) 53. Andrault et al. (2003) 54. Liu et al. (1999) 55. Sinogeikin et al. (2004) 56. Wentzcovitch et al. (2004) 57. Shim & Duffy (2000) 58. Fiquet et al. (2000) 59. Kiefer et al. (2002) 60. Kubo & Akaogi (2000) 61. Thompson et al. (1996) 62. Jackson et al. (1990) 63. Jacobsen et al. (2002) 64. Stolen et al. (1996)

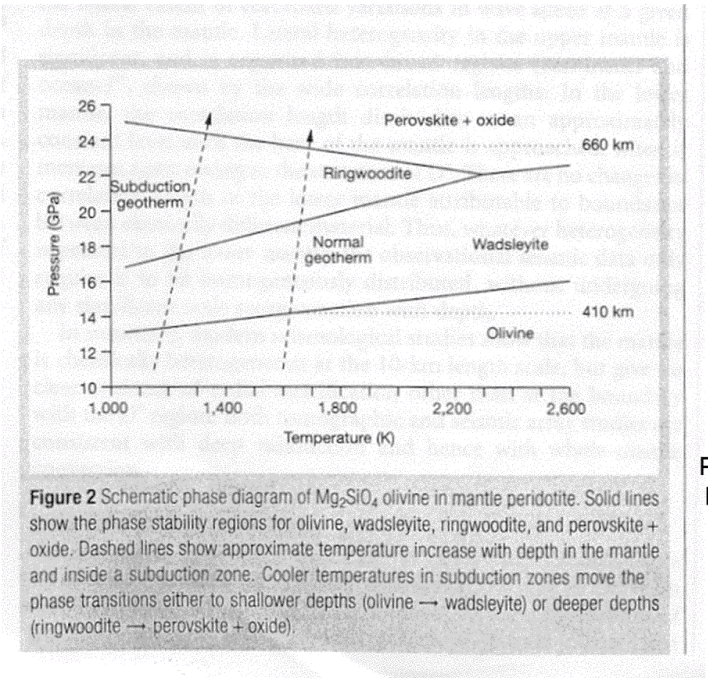

Figure 2 Schematic phase diagram of Mg_2SiO_4 olivine in mantle peridotite. Solid lines show the phase stability regions for olivine, wadsleyite, ringwoodite, and perovskite + oxide. Dashed lines show approximate temperature increase with depth in the mantle and inside a subduction zone. Cooler temperatures in subduction zones move the phase transitions either to shallower depths (olivine → wadsleyite) or deeper depths (ringwoodite → perovskite + oxide).

$(Mg,Fe)_2SiO_4$ System

Olivine

↓ 410 km

Wadsleyite (β phase)

↓ 520 km

Ringwoodite (γ phase)

↓ 660 km

Perovskite $(Mg,Fe)SiO_3$ + Ferropericlase $(Mg,Fe)O$

--All necessary aggregate elastic properties and their P and T derivatives are measured

--Good agreement across different labs using different techniques

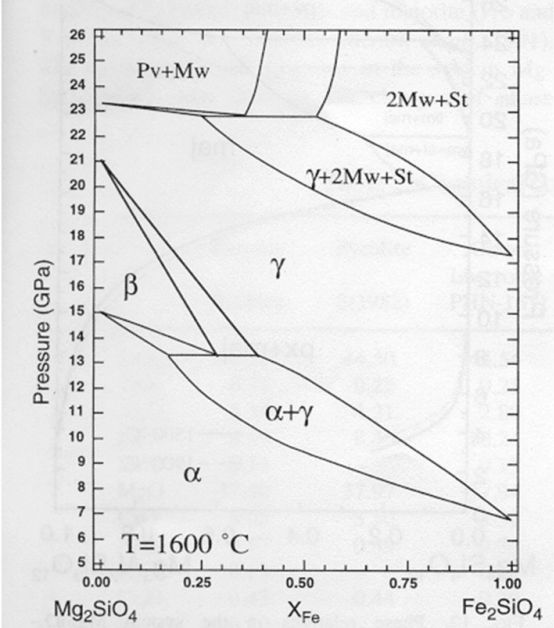

FIG. 10. Phase diagram in the system Mg_2SiO_4-Fe_2SiO_4 at 1600°C. Data sources are KATSURA and ITO (1989), ITO and TAKAHASHI (1989), FEI *et al.* (1991), and AKAOGI *et al.* (1998).

Seismic Discontinuities:

-- Identification with particular phase transition(s)

i.e. Does the post-spinel transition occur at the correct pressure for expected mantle temperatures?

Alternatively, can we constrain temp. at 660 km from Clapeyron slope?

--How well do seismic and laboratory characteristics match?

Seismically observed depth interval vs. petrological thickness

Discontinuity topography vs. Clapeyron slope of the transition

Amplitude of discontinuity vs. expected change in sound velocities at P-T

Fine structure (splitting, non-linearity, etc.)

Gradient in transition zone compared with mineral velocity-depth trajectories

Phase	Density (g/cm^3)	Bulk Modulus, K (GPa)	Rigidity, μ (GPa)	V_P (km/s)	V_S (km/s)
α olivine Mg_2SiO4	3.222	129	82	8.60	5.05
β wadseyite Mg_2SiO4	3.47	174	114	9.69	5.73
γ ringwoodite Mg_2SiO4	3.56	184	119	9.81	5.78
Perovskite ($MgSiO_3$)	3.81	253	175	11.29	6.78
Periclase (MgO)	3.59	163	131	9.70	6.04

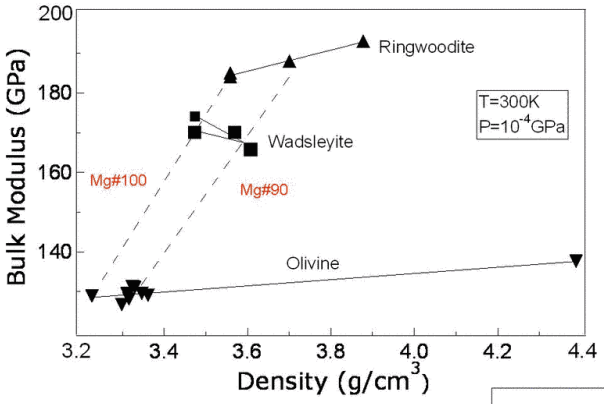

Aggregate elasticity of the $(Mg,Fe)_2SiO_4$ system

Effects of composition and structure

Elastic modulus – density systematics for $(Mg,Fe)_2SiO_4$ system (Birch plots).

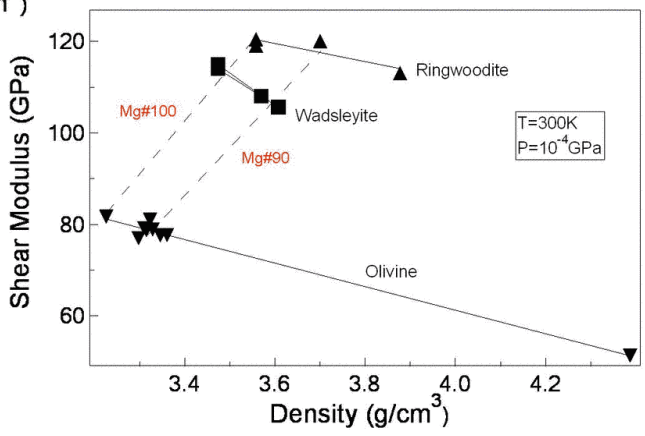

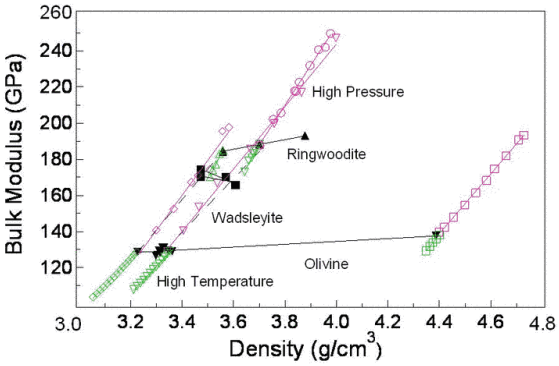

Birch Plots:

Effects of pressure and temperature

Bulk modulus: Pressure, temperature, structure effects follow a common trend

Shear modulus: Pressure, temperature, structure effects show marked variability

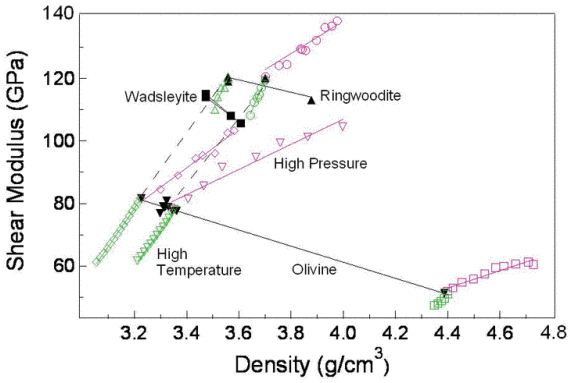

Velocity changes associated with Olivine (X_{Fe}=0.1) phase transformations at ambient P and T

	$\Delta\rho$ (%)	ΔV_P (%)	ΔV_S (%)
α(0 → 14GPa)	10%	10%	6%
α (300 → 1700 K)	-5%	-9%	-11%
$\alpha \rightarrow \beta$	8%	13%	14%
AK135 410 km	--	**3.7%**	**4.3%**
$\beta \rightarrow \gamma$	3%	1%	1%
γ → Pv+Per	5%	8%	11%
AK135 660 km	--	**5.8%**	**6.2%**

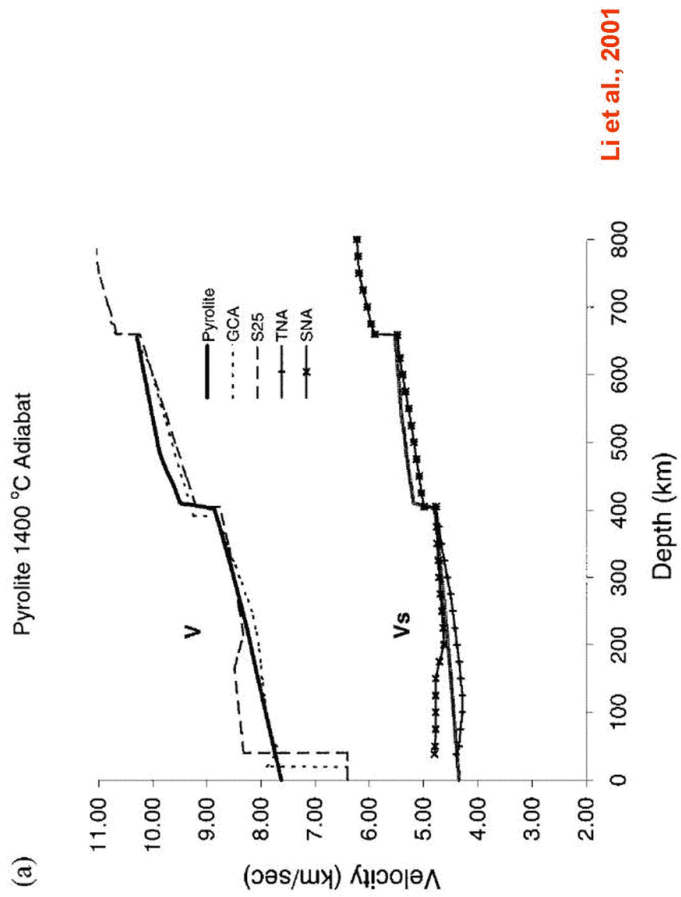

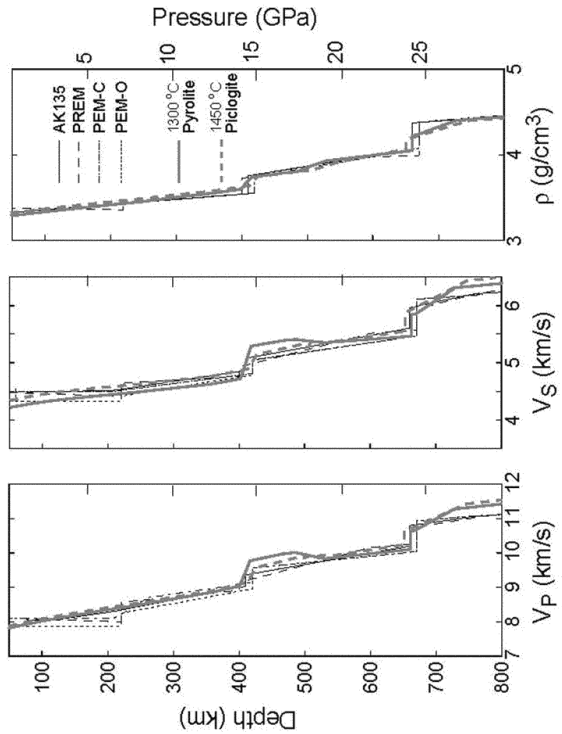

Cammarano et al. 2003

Elasticity of San Carlos olivine to 8 GPa and 1073 K

Wei Liu, Jennifer Kung, and Baosheng Li
Mineral Physics Institute, State University of New York, Stony Brook, New York, USA

Received 13 May 2005; accepted 22 July 2005; published 16 August 2005.

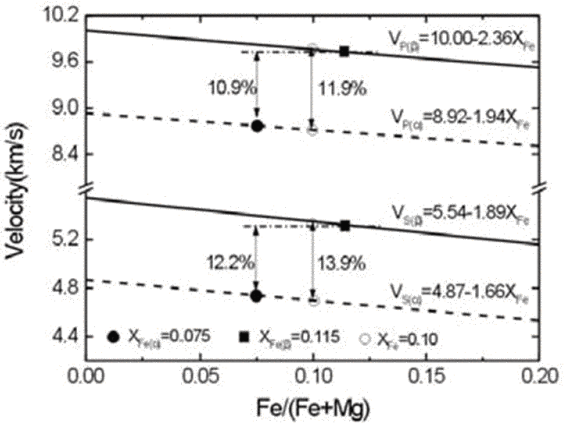

Increases in V_P and V_S range from **4-6%** in seismic velocity models

Mineral elasticity studies are in broad agreement that the velocity jump from α to β phase at high P-T is **12-14%** (cf: Duffy et al., 95)

The fraction of olivine required at 410 km depth to satisfy seismic data is **40-50% (cf: the olivine abundance in pyrolite is 60%)**

Impedance contrast across the 410-km discontinuity from PP and SS Precursors

Chambers et al., *JGR*, 05

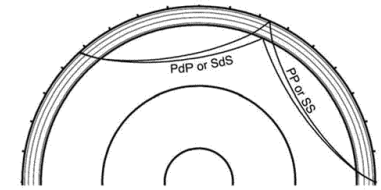

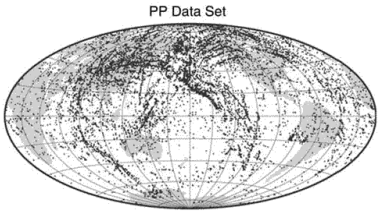

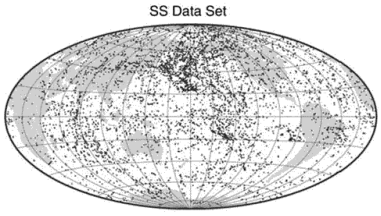

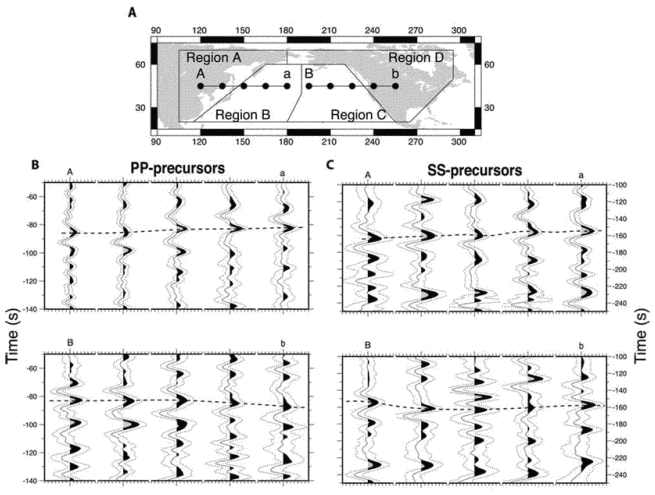

Impedance contrast across the 410-km discontinuity from PP and SS Precursors

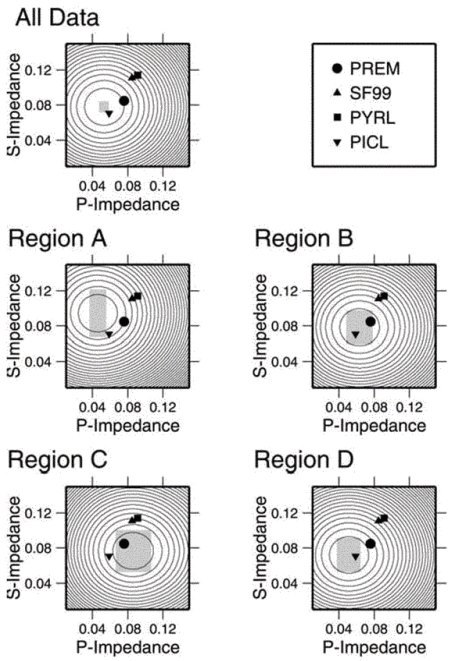

Chambers et al., *JGR*, 05

Chambers et al. 2005	
P wave impedance	0.053(5)
S wave impedance	0.078(6)
Shearer and Flanagan, 1999	
P wave impedance	0.085
S wave impedance	0.111
Pyrolite	
P wave impedance	0.092
S wave impedance	0.114
Olivine depleted	
P wave impedance	0.059
S wave impedance	0.071

Reconciling mineral physics evidence at 410-km with petrological evidence for olivine-rich pyrolite at shallow mantle depths.

-- **The phase transformation produces a non-linear compositional gradient** resulting in seismic underestimates of olivine abundance at 410 km (Helffrich and Wood, 96, Stixrude 97, Gaherty et al. 99)

-- Related issue: Fe partitioning changes between α and β phases and residual mantle components (garnet) must be accounted for (Irifune and Isshiki, 1998)

-- **Hydrated transition zone**. β phase is enriched in water compared to α phase, reducing seismic velocity contrast.

-- **Mantle at 410-km depth is olivine depleted** compared with uppermost mantle.

Other considerations:

-- Phase transition width versus seismically observed thickness

-- Relationship between seismic topography and phase transition Clapeyron slope.

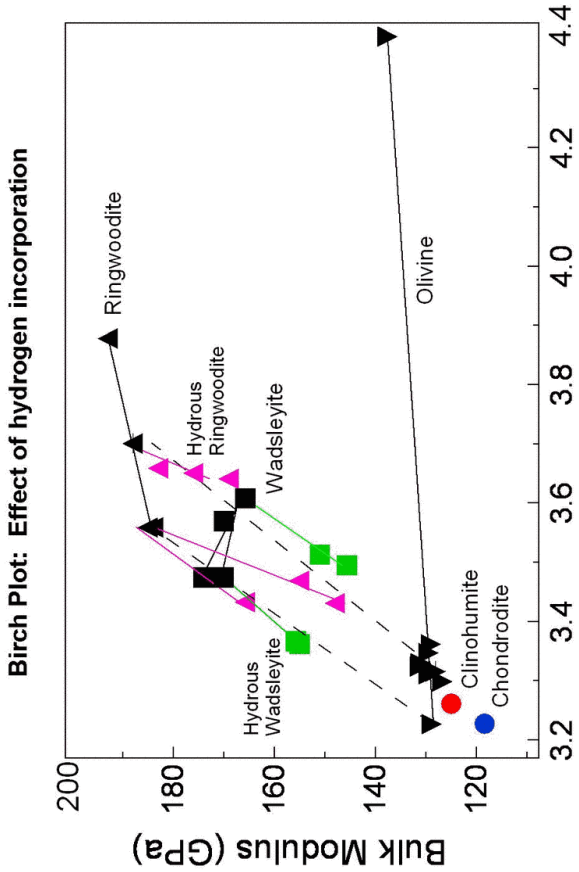

References for hydrous $(Mg,Fe)_2SiO_4$:

Wang et al., 2003; Inoue et al., 1998, 2004; Yusa et al., 2000; Jacobsen et al., 2004; Yusa and Inoue, 1997; Smyth et al., 2004

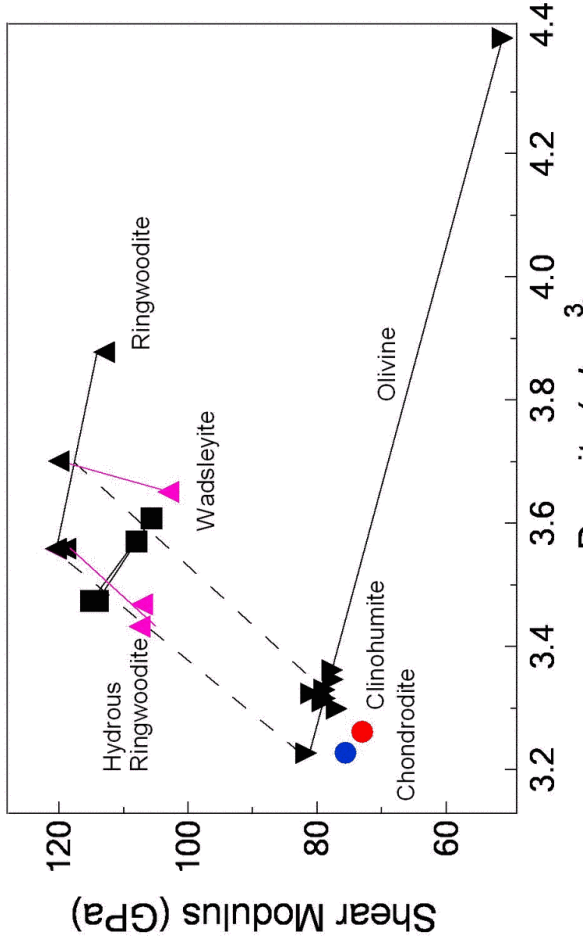

References for hydrous Ringwoodite:

Wang et al., 2003; Inoue et al., 1998, 2004; Jacobsen et al., 2004

Water contents of 1.5-2 wt% in Wadsleyite are required to reconcile mineral physics data with seismology.

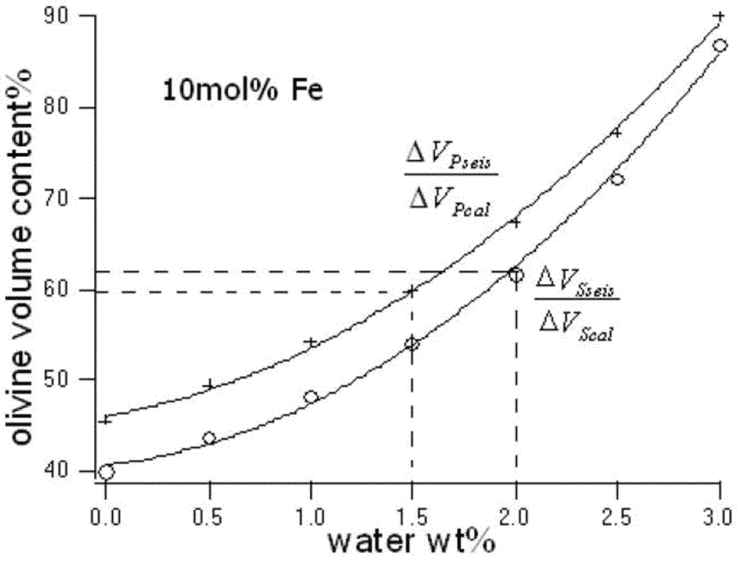

Effect of H_2O incorporation on K, G obtained using Birch's Law

Estimates of mantle water content:

Wadsleyite capacity at 410 P-T (Hirschmann et al 05)	1-2 wt %
MORB source	<0.02 wt %
OIB source	<0.07 wt %
Width of 410 (Wood 95; van der Meidje 03)	0.02-0.07 wt %
Transition zone conductivity (Huang et al 05)	0.1-0.2 wt %

Other factors:

Upper mantle capacity (Hirschmann et al 05)	>0.04 wt %
Partial melt? (Bercovici and Karato 03)	

Olivine does not exist in isolation….

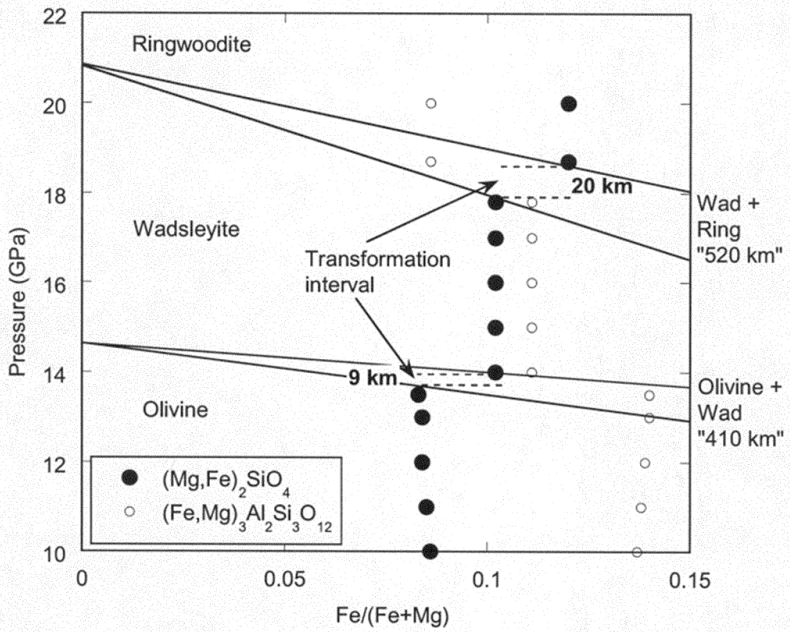

The Fe-Mg distribution coefficient for garnet-wadsleyite is lower than for garent-olivine

Compressional velocity across the α-β transformation accounting for non-linear yield of the high-pressure phase

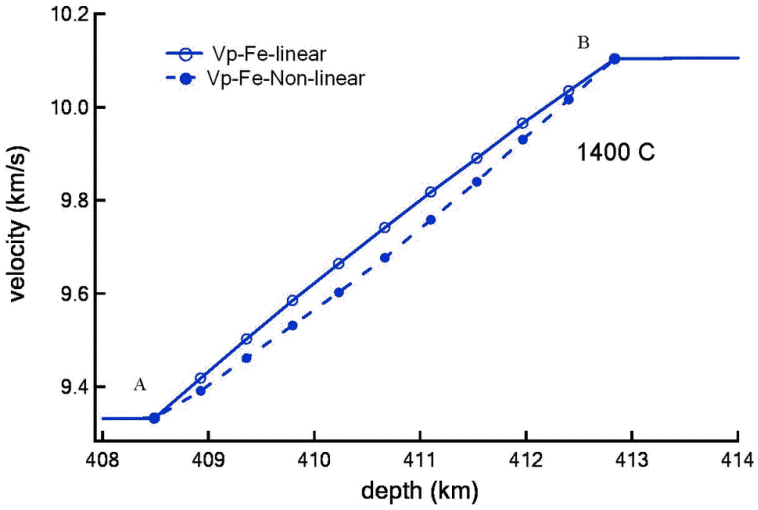

Frost (2003): internally consistent thermodynamic model for $(Mg,Fe)_2SiO_4$ incorporating non-ideality of mixing.

For α-β transformation: pressure interval of 5-6 km; nearly linear mineral yields

Katsura et al., *JGR*, 2005

Study of olivine-wadsleyite transformation in $(Mg,Fe)_2SiO_4$ at 1600 K and 1900 K

Thickness of olivine-wadsleyite transformation in a pyrolite composition is 7-13 km.

Short period seismic wave observations indicate maximum thickness <5 km.

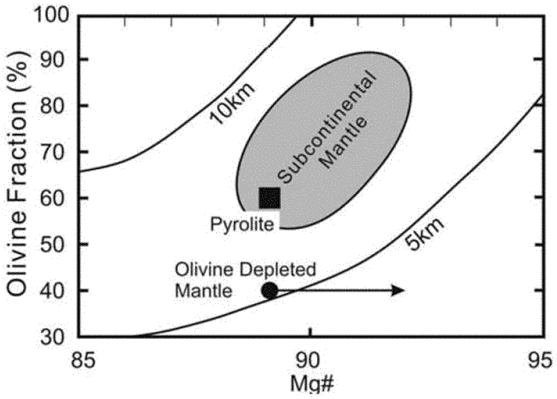

Effect of H_2O on transition width?

"An upper mantle in the region of the 410 km discontinuity with about 40% olivine and an Mg# of at least 89 can possibly explain both the transition thickness and velocity perturbation at the 410 km discontinuity." Katsura et al. 2005

Factors affecting seismic wavespeed variations:

Temperature, pressure, anelasticity, chemistry

Karato and Karki, 2001

$$\left(\frac{\partial \ln V_S}{\partial \ln V_P}\right)_T$$

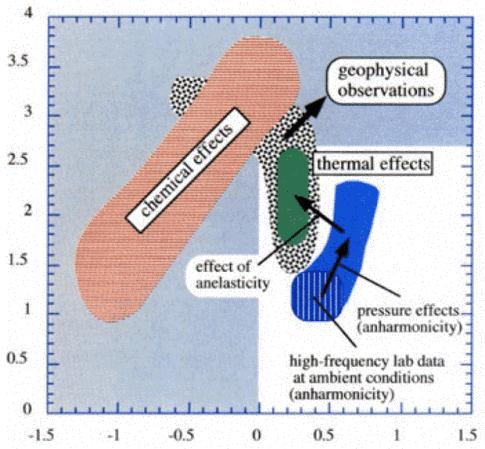

Table 2. Partial Derivatives Corresponding to Changes in Chemical Composition[a]

	X=Fe/(Fe+Mg)[b]	X=Si/(Si+Mg)[c]	X=Ca/(Ca+Mg)[d]
$d\log\rho/dX$	0.5±0.2	0.040	0.045
$d\log V_s/dX$	-0.5±0.1	0.015	0.082
$d\log V_p/dX$	-0.4±0.1	0.012	0.020
$d\log V_\phi/dX$	-0.2±0.1	0.014	-0.021

[a] Simultaneous changes in chemical compositions of more than two elements are not considered for simplicity.
[b] Values for olivine and (Mg,Fe)O
[c] Values for change in $MgO/MgSiO_3$
[d] Values for change in $CaSiO_3/MgSiO_3$

$$\left(\frac{\partial \ln \rho}{\partial \ln V_S}\right)_T$$

Compositional effect on the compressional, shear and bulk velocity heterogeneity parameters in different solid solution series calculated at ambient conditions

Solid **solution series**	X	$\partial \ln v_P/\partial X$	$\partial \ln v_S/\partial X$	$\partial \ln v_B/\partial X$	$\partial \ln v_S/\partial \ln v_P$	$\partial \ln v_P/\partial \ln \rho$	$\partial \ln v_S/\partial \ln \rho$	$\partial \ln v_B/\partial \ln \rho$
Forsterite - fayalite	Fe/(Mg+Fe)	**-0.24** (1)	**-0.37** (1)	-0.14 (1)	1.54 (8)	-0.67 (5)	-1.1 (1)	-0.37 (4)
Al-Garnet (Ca/Mg = constant)	Fe/(Mg+Fe)	**-0.09** (1)	**-0.08** (1)	-0.09 (2)	0.9 (1)	-0.52 (5)	-0.48 (5)	-0.44 (4)
Al-Garnet (Ca/Fe = constant)	Fe/(Mg+Fe)	**-0.05** (1)	**-0.08** (1)	-0.08 (1)	1.6 (3)	-0.26 (3)	-0.40 (4)	-0.39 (5)
Orthoenstatite - orthoferrosilite	Fe/(Mg+Fe)	**-0.21** (2)	**-0.30** (4)	-0.14 (2)	1.4 (3)	-0.92 (9)	-1.3 (3)	-0.59 (6)
Diopside - hedenbergite	Fe/(Mg+Fe)	**-0.09** (1)	**-0.15** (2)	-0.04 (1)	1.7 (3)	-0.79 (8)	-1.4 (1)	-0.37 (4)
Wadsleyite - β-Fe_2SiO_4	Fe/(Mg+Fe)	-0.37 (5)	-0.52 (6)	-0.23 (6)	1.4 (2)	-1.2 (2)	-1.6 (2)	-0.8 (4)
Ringwoodite - γ-Fe_2SiO_4	Fe/(Mg+Fe)	**-0.18** (3)	**-0.28** (4)	-0.09 (5)	1.6 (3)	-0.48 (4)	-0.74 (5)	-0.26 (5)
Periclase - wüstite	Fe/(Mg+Fe)	-0.46 (5)	**-0.74** (7)	-0.27 (2)	1.6 (2)	-1.0 (1)	-1.5 (2)	-0.35 (4)
Mg,Fe-Opx - Mg-Tschermak	$Al^{VI}/(Al^{VI}+Mg+Fe)^*$	0.24 (4)	0.13 (4)	0.33 (6)	0.6 (5)	7 (2)	4 (2)	10 (4)
Majorite - pyrope	$Al/(Al+Mg^{VI}+Si^{VI})^*$	0.03 (1)	0.04 (1)	0.02 (1)	1.3 (3)	1.2 (1)	1.5 (1)	---
Al-Garnet (Fe/Mg = constant)	Ca/(Mg+Ca)	0.03 (1)	0.08 (1)	---	2.7 (6)	-1.6 (2)	-3.7 (4)	---

$^*Al^{VI}$, Mg^{VI}, Si^{VI} are in octahedral coordination.
--- Unresolved parameter.

References
Orthoenstatite - orthoferrosilite: *Kumazawa* [1969]; *Frisillo and Barsch* [1972]; *Weidner et al.* [1978]; *Bass and Weidner* [1984]; *Duffy and Vaughan* [1988]; *Webb and Jackson* [1993]; *Jackson et al.* [1999].
Diopside - hedenbergite: *Kandelin and Weidner* [1988]; *Collins and Brown* [1998]; *Isaak and Ohno* [2003].
Wadsleyite - β-Fe_2SiO_4: *Sawamoto et al.* [1984]; *Sinogeikin et al.* [1998]; *Zha et al.* [1998].
Ringwoodite - γ-Fe_2SiO_4: *Weidner et al.* [1984]; *Rigden and Jackson* [1991]; *Rigden et al.* [1992]; *Sinogeikin et al.* [1997]; *Jackson et al.* [2000]; *Sinogeikin et al.* [2003 a].
Majorite - pyrope: *Bass and Kanzaki* [1990]; *Yeganeh-Haeri et al.* [1990]; *O'Neill et al.* [1991]; *Sinogeikin and Bass* [2000]; *Sinogeikin et al.* [2002].
Periclase – wüstite: *Sinogeikin and Bass* [2000]; *Jacobsen et al.* [2002].

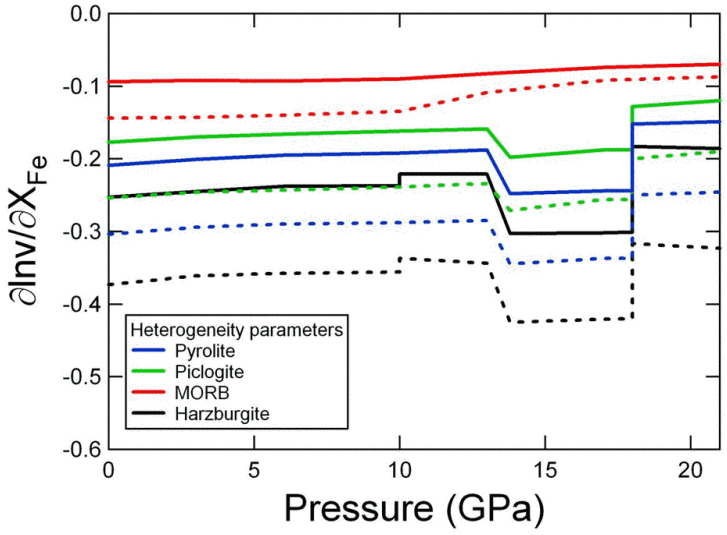

Speziale and Duffy, 2005

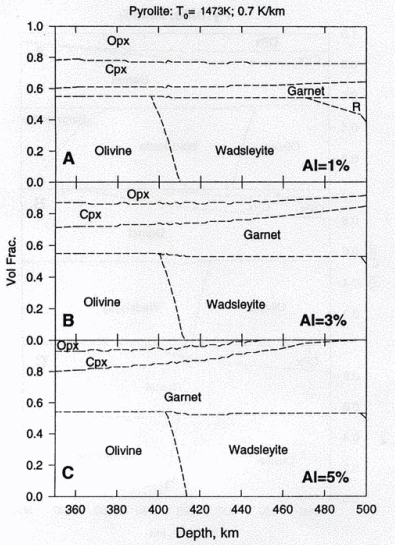

Figure 5. Volume fractions of stable phases with varying Al contents as shown (ratio of all other cations remains constant). For the low Al (1 cation %) model, pyroxenes dominate the non-olivine component. Note that in this plot the higher pressure field for pyroxenes is not shown, which should include wadsleyite/ringwoodite plus stishovite. Note gradual increase in garnet as Al content increases.

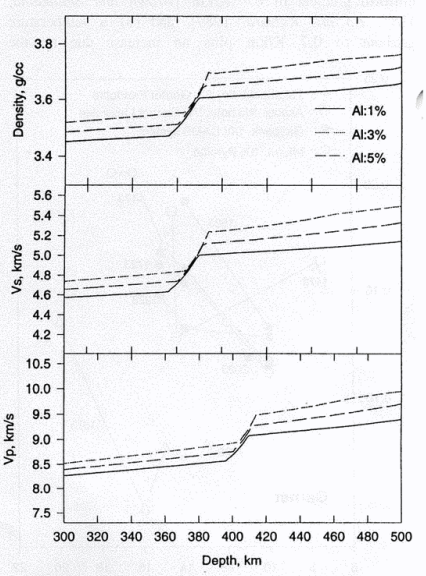

Figure 6. Density (upper), Vs (middle), and Vp (lower) of pyrolite with various Al contents. All models follow a geotherm whose zero pressure temperature is 1473 K. Higher Al models have high density and velocities because garnets have higher shear and bulk moduli than pyroxenes.

Weidner and Wang